Applied Clay Science 161 (2018) 482–493

Contents lists available at ScienceDirect

Applied Clay Science

journal homepage: www.elsevier.com/locate/clay

Research paper

Gypsum precipitation enhanced by electrokinetic method and porewater chemistry in compacted montmorillonite

Shingo Tanaka

Division of Energy and Environmental Systems, Faculty of Engineering, Hokkaido University, Kita 13 Nishi 8, Kita-ku, Sapporo, Hokkaido 060-8628, Japan

ARTICLE INFO

Keywords:
Cement-bentonite interactions
Reactive transport model
Porewater chemistry
Gypsum precipitation
Electromigration
Diffusion

ABSTRACT

An understanding of chemical reactions in bentonite is important in completing a reliable safety assessment of the geological disposal of radioactive waste. In the present study, porewater chemistry and calcium reactivity in a compacted Na/Ca-mixed montmorillonite is explored through a gypsum precipitation reaction enhanced using an electrokinetic method. Results showed that $CaSO_4$ was sparsely precipitated as gypsum in up to 300-μm aggregates, and grew into the montmorillonite texture. A threshold ionic equivalent fraction of calcium, X_{Ca}, of the Na/Ca-mixed montmorillonite in the gypsum precipitation was experimentally found to be within a range between $X_{Ca} = 0.1$ and $X_{Ca} = 0.25$ under a dry density of 1.0 kg/dm^3 saturated with 0.5 M Na_2SO_4 solution. The saturation indices of gypsum for specimens following the precipitation experiments were evaluated based on a model including anion exclusion and cation exchange (Gains-Thomas selectivity coefficients, K_{GT}) between the montmorillonite and interparticle solution using the PHREEQC code. Gypsum precipitation regions obtained from the precipitation experiments are in good agreement with regions in which the saturation indices are greater than zero when assuming $K_{GT} = 200$, which is much greater than the $K_{GT} = 4.9$ reported from the batch experiment. The greater K_{GT} value implied in this study indicates that the thermodynamic properties of confined solutions are different from those of diluted or bulk solutions. The reason for the K_{GT} deviation remains unresolved; however, the precipitation tendency of gypsum may be explained by a model including anion exclusion and cation exchange between the montmorillonite and the interparticle solution when an adequate K_{GT} value is used in the calculation.

1. Introduction

When assessing the geological disposal of radioactive wastes, it is important to evaluate long-term interactions between clay materials and other engineered barriers. In this regard, cement/clay interactions (Gaucher and Blanc, 2006; Savage et al., 2007) and iron/clay interactions (Bildstein et al., 2006; Savage et al., 2010) have been investigated intensely throughout the world. The reactive transport of chemical species among these barriers (Watson et al., 2009; Wilson et al., 2015) and porewater compositions in clay materials (Gaucher et al., 2009; Wersin et al., 2016) have been predicted using geochemical calculation codes including cation exchange reactions between clay materials and porewater in compacted systems. A selectivity coefficient of the Gaines-Thomas convention, K_{GT} (Gaines and Thomas, 1953), obtained from diluted systems, such as a batch experiment, has often been used in the modeling of cation exchange reactions in compacted systems because of the experimental difficulty in obtaining in-situ K_{GT}. The applicability of the selectivity and other coefficients obtained from diluted systems to compacted systems is among the most important questions in radioactive waste disposal.

Sodium bentonite is widely used as an engineered barrier, including Kunigel V1 (Oda and Shibata, 1999) and MX-80 (Karnland, 2010). In cement/clay interactions, calcium ions arising from dissolution of cementitious materials will diffuse in the sodium bentonite accompanied by cation exchange and secondary mineral precipitation. Therefore, it is important to elucidate the calcium reactivity in Na/Ca-mixed compacted bentonite. In this context, precipitation of secondary minerals will decrease the clay porosity, referred to as clogging, sealing (Gaucher and Blanc, 2006) and/or cementation (Steefel and Lictner, 1994). Clogging of natural argillite porosity resulting from newly formed minerals including calcium silicate hydrates (C-S-H), calcite and gypsum is suggested in long-term in-situ experiments of cement/clay interactions (De Windt et al., 2008; Gaboreau et al., 2011; Techer et al., 2012). In addition, the impacts of cement water on the diffusion of compacted clay has been investigated in a laboratory experiment (Melkior et al., 2004), suggesting that the tritium water (HTO) effective diffusion coefficient decreases over a 12-month period because of clogging.

Although calcium precipitation is suggested in-situ (De Windt et al.,

E-mail address: tanaka-shingo@eng.hokudai.ac.jp.

https://doi.org/10.1016/j.clay.2018.05.011
Received 5 January 2018; Received in revised form 10 May 2018; Accepted 11 May 2018
Available online 26 May 2018

2008; Gaboreau et al., 2011; Techer et al., 2012) and in laboratory experiments (Melkior et al., 2004), little is known regarding the reaction mechanisms involving calcium precipitation in compacted bentonite, because of its micro- or nano-scale pore structures (Kozaki et al., 1998; Melkior et al., 2009) and strong negative charge. In this regard, diffusion mechanisms of anions and cations in compacted bentonite have been intensely investigated and discussed. Models incorporating different types of pore spaces such as interlayer between montmorillonite sheets, interparticle space among montmorillonite stacks and external surface are proposed to explain ion diffusion in bentonite (Bourg et al., 2008; Glaus et al., 2010; Kozaki et al., 2001; Tachi and Yotsuji, 2014; Tournassat and Appelo, 2011; Van Loon et al., 2007). The selectivity coefficient was introduced to evaluate cation exchange reactions between clays and interparticle solutions in compacted bentonite (Glaus et al., 2007; Tachi and Yotsuji, 2014). Models introducing the membrane behavior of clay have been proposed based on the Donnan effect (Birgersson, 2017; Birgersson and Karnland, 2009; Leroy et al., 2006; Muurinen et al., 2004). Application of the concepts including multiple porosities and/or the Donnan effect to the models addressing reactive transport and porewater composition is becoming increasingly popular in recent studies (Alt-Epping et al., 2018; Alt-Epping et al., 2014; Wersin et al., 2016; Zheng and Samper, 2015). In contrast, there are few experimental options, such as long-term diffusion and permeability experiments, to investigate the chemical reactions in bentonite, which makes it difficult to understand its reactive transport and porewater chemistry.

Because of the quite low hydraulic conductivity and diffusional mass transport in clay materials, some in-situ and laboratory experiments regarding clay alterations have taken longer than one year (Melkior et al., 2004; Techer et al., 2012). For the same reason, it is quite difficult to verify the results of long-term evaluations between clay materials and other engineered barriers. In contrast, electrokinetic methods have an advantage of enhancing ion migration in bentonite and in turn drastically decreasing the test duration. Thus far, this method has been applied in many ways to compacted clay materials as follows: (1) evaluation of diffusion coefficients over a short duration (Maes et al., 1999), (2) investigation of chemical speciation (Beauwens et al., 2005), (3) determination of charge carriers (Higashihara et al., 2008), and (4) discussion regarding migration pathways of ions (Tanaka et al., 2008; Tanaka et al., 2011). In addition to these findings, the method has a possibility of enhancing chemical reactions as anions migrate in the opposite direction from that of cations under an electric potential gradient.

The purpose of this study was to investigate the porewater chemistry and calcium reactivity in compacted Na/Ca-mixed montmorillonite from a gypsum precipitation reaction enhanced by electrokinetic method. First, electromigration experiments of $^{22}Na^+$, $^{45}Ca^{2+}$, $^{35}SO_4^{2-}$ and HTO were conducted to determine migration coefficients (velocities, dispersion coefficients, transport numbers, etc.) under the same experimental conditions as those of the precipitation experiments. Based on these migration coefficients, an optimal condition for gypsum precipitation was determined. Second, the method was applied to gypsum precipitation in the compacted montmorillonite. An ionic equivalent fraction of calcium (X_{Ca}) in the montmorillonite was chosen as a variable for gypsum precipitation rather than the Na_2SO_4 concentration, because basal spacing in the montmorillonite at a dry density of 1.0 kg/dm^3 saturated with deionized water does not change with respect to X_{Ca} (Kozaki et al., 2010). In contrast, changing the Na_2SO_4 concentration in the montmorillonite will result in a drastic change in the microstructural characteristics. Therefore, the initial concentration was set to be 0.5 M Na_2SO_4 for all the precipitation experiments, and then a threshold X_{Ca} for gypsum precipitation was experimentally determined. Third, X-ray diffraction analysis (XRD) and electron probe X-ray microanalysis (EPMA) were conducted on specimens following the precipitation experiments to identify the mineral species, size, and form of the precipitates. Finally, saturation indices of gypsum were estimated using the PHREEQC code to discuss the tendency of gypsum precipitation.

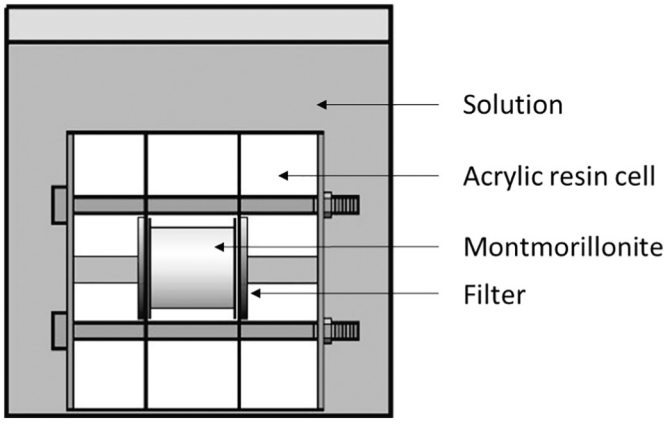

Fig. 1. Experimental apparatus for saturation of montmorillonite specimens. In the case of the Na/Ca-mixed montmorillonite, deionized water was used as solution. In the case of the Na montmorillonite, 0.5 M Na_2SO_4 solution labeled by S-35 radiotracer was used. The dry density was set as 1.0 kg/dm^3 in all experiments.

2. Experimental methods and materials

2.1. Preparation of montmorillonite specimens

Homoionized Na- and Ca-montmorillonite purified from Kunipia-F were mixed to obtain Na/Ca-montmorillonite mixtures. Detailed preparation procedures are described elsewhere (Kozaki et al., 1999). The ionic equivalent fraction of calcium, X_{Ca}, was set as 0.10, 0.25, 0.50, and 0.75. These were compacted as specimens 20 mm in diameter and 20 mm in length, with a dry density of 1.0 kg/dm^3. The specimens were immersed in deionized water as shown in Fig. 1. The containers with the specimens and water were maintained in a vacuum desiccator for 15 min to prompt water saturation. Following this, these were maintained for > 30 days to complete saturation. The Na-montmorillonite was compacted with a dry density of 1.0 kg/dm^3, and saturated with 0.5 M Na_2SO_4 solution labeled by the S-35 radioisotope in the same manner as shown in Fig. 1. The minimum saturation period (30 days) was predicted analytically based on an apparent diffusion coefficient of SO_4^{2-} ions in Na montmorillonite at a dry density of 1.0 kg/dm^3 saturated with 0.5 M Na_2SO_4 under the same initial and boundary conditions as shown in Fig. 1.

After saturation, the initial concentrations of Na (including exchangeable Na^+ in the montmorillonite, free Na^+, and $NaSO_4^-$ as an ion-pair) and SO_4 (including free SO_4^{2-} and $NaSO_4^-$) in the montmorillonite were determined. The saturated specimen was sliced, and all the Na and SO_4 was extracted using 1 M NH_4Cl solution. The Na concentration was determined by inductively coupled plasma atomic emission spectroscopy (ICP-AES), and the SO_4 concentration was determined from S-35 radioactivity measured using a liquid scintillation counter.

2.2. Electromigration of $^{22}Na^+$, $^{45}Ca^{2+}$, $^{35}SO_4^{2-}$ and HTO

Electromigration experiments of $^{22}Na^+$, $^{45}Ca^{2+}$, $^{35}SO_4^{2-}$, and HTO were conducted to obtain the migration coefficients of each species. A small amount of tracer ($^{22}NaCl$, $^{45}CaCl_2$, $Na_2{}^{35}SO_4$, or HTO) was applied to the contact surface of the montmorillonite specimens. During the experiments of the Na/Ca-mixed montmorillonite with different ionic equivalent fractions of calcium (X_{Ca} = 0.25, 0.50, and 0.75), $^{22}Na^+$, $^{45}Ca^{2+}$, and HTO were used as tracers. During the experiments of Na-montmorillonite saturated with 0.5 M Na_2SO_4 solution, $^{22}Na^+$,

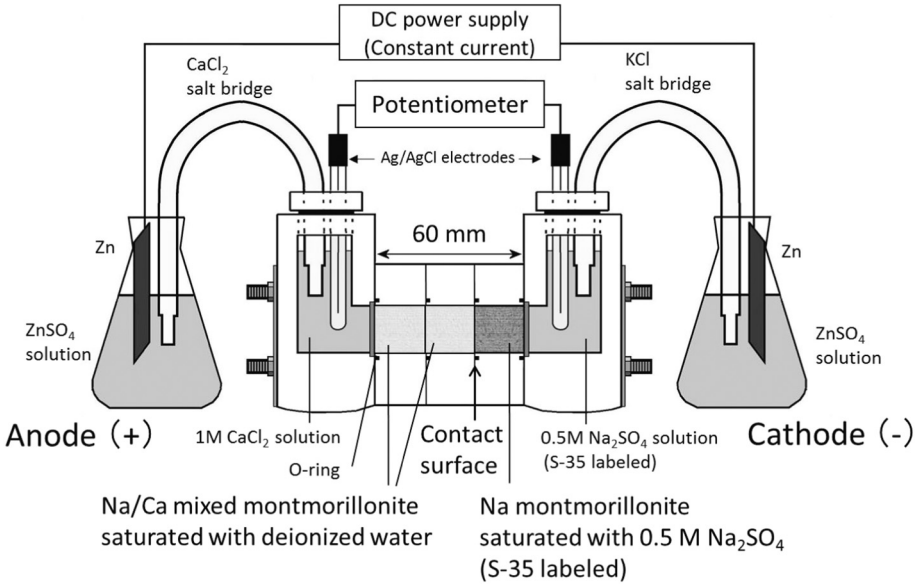

Fig. 2. Experimental apparatus for gypsum precipitation. The montmorillonite specimens consisted of two Na/Ca-mixed montmorillonite saturated with deionized water with the same X_{Ca} for each test, and Na-montmorillonite saturated with 0.5 M Na_2SO_4 solution in the series.

$^{35}SO_4^{2-}$, and HTO were used as tracers. A constant current of 5 mA was applied to the specimens for 86,400 s. The detailed experimental procedures are described elsewhere (Tanaka et al., 2011). Following the experiment, the montmorillonite specimens were sliced, and the concentration profiles of each tracer were obtained from the radioactivities of each slice measured using a gamma counter or a liquid scintillation counter.

2.3. Gypsum precipitation enhanced via the electrokinetic method

The experimental apparatus for gypsum precipitation is shown in Fig. 2. The montmorillonite specimens were composed of two Na/Ca-mixed montmorillonite with the same X_{Ca} saturated with deionized water, and Na-montmorillonite saturated with 0.5 M Na_2SO_4 labeled by S-35 in the series. Four experiments were conducted with a different X_{Ca} (0.10, 0.25, 0.50, and 0.75). On each side of the montmorillonite specimens, the cells containing 1 M $CaCl_2$ or 0.5 M Na_2SO_4 solution labeled by S-35 were connected to $Zn/ZnSO_4$ electrodes using a $CaCl_2$ or KCl salt bridge to mitigate changes in the concentrations and pH in the cells. A constant current of 5 mA was applied to the montmorillonite specimens for 86,400 s at a temperature of 298 K. The electric potential difference between the cells was measured using the reference Ag/AgCl electrodes during the experiment. After applying the constant current, the montmorillonite specimens were sliced to 0.5 mm, and then the concentrations of total Na (including exchangeable Na^+ in the montmorillonite, free Na^+, and $NaSO_4^-$ as an ion-pair), total Ca (including exchangeable Ca^{2+} in the montmorillonite, free Ca^{2+}, $CaSO_4^0$ as an ion-pair, and precipitated $CaSO_4$), mobile SO_4 (including free SO_4^{2-}, $NaSO_4^-$, and $CaSO_4^0$), and precipitated SO_4 (as $CaSO_4$) in each slice were determined. For separation of the mobile and precipitated SO_4 concentrations, the mobile $^{35}SO_4$ in each slice was extracted by adding 10 mL of saturated $CaSO_4$ solution (S-35 free) as an extractant. These were shaken for a short time (1 h) so as not to dissolve the precipitated $Ca^{35}SO_4$. Following centrifugation and 0.45-μm filtration, the amount of mobile SO_4 in each slice was determined from the S-35 radioactivities in the filtrated solution. Precipitated $Ca^{35}SO_4$ in the residues was dissolved by adding 1 M NH_4Cl solutions, and these were shaken for 24 h. Following the centrifugation and 0.45-μm filtration, the amount of precipitated SO_4 in each slice was determined from the S-35 radioactivity in the filtrated 1 M NH_4Cl solution. During the process of precipitated SO_4 determination, the amount of mobile $^{35}SO_4$ in the wet residue was corrected using a volume, which was determined from a weight difference between the slice and the residue, and the S-35 radioactivity in the saturated $CaSO_4$ solution which was previously determined during the process of mobile $^{35}SO_4$ extraction. The total Na and Ca in each slice was extracted and dissolved by using 1 M NH_4Cl solution. Following the centrifugation and 0.45-μm filtration, the concentrations of Na and Ca were determined using ICP-AES.

2.4. XRD and EPMA analysis

Following the gypsum precipitation experiment (S-35 free) at $X_{Ca} = 0.75$, the montmorillonite specimens were sliced to 1 mm, and vacuum-dried at room temperature. Dried slices of 0.0–1.0 mm and 6.0–7.0 mm from the contact surface were broken into several pieces. Among them, a large piece was chosen and saturated with a resin (Struers, EpoFix Resin) under vacuum conditions. The solidified piece was polished using SiC polishing paper (particle size of 4 μm). Following carbon vapor deposition, the polished surface (perpendicular to the x direction) was analyzed using EPMA (JEOL, JXA-8530F) to obtain backscattered electron (BSE) images and elemental maps. The observation was conducted using a probe current of 4.5×10^{-8} A and an acceleration voltage of 15 kV. The remaining pieces and the other slices were crushed in an alumina mortar and sieved to obtain powder samples < 75 μm. These powdered samples were analyzed using XRD (Rigaku, RINT-2000) to identify mineral species. The XRD analysis was conducted with CuKα, a tube voltage of 40 kV, a tube current of 30 mA, a step width of 0.05 degrees and a measurement time during each step of 2 s.

3. Results and discussion

3.1. Initial concentrations of Na and SO_4

Fig. 3 shows the initial equivalent concentrations of Na and SO_4 per unit of dry montmorillonite as a function of distance from the center of the montmorillonite specimen at a dry density of 1.0 kg/dm^3 saturated with 0.5 M Na_2SO_4 solution. The specimen was in contact with the external solution on each side. The dashed line indicates the cation exchange capacity (CEC) of the montmorillonite (1.05 eq/kg). The dashed-two dotted line and dashed-dotted line indicate the expected Na and SO_4 concentrations, respectively, estimated based on the

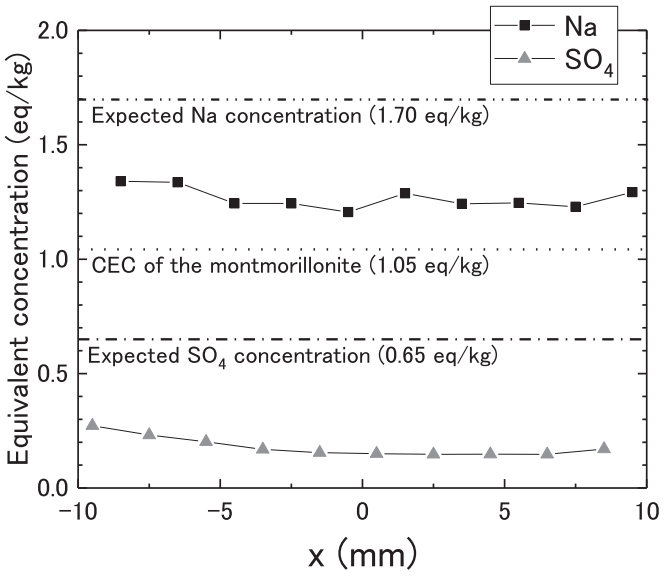

Fig. 3. Initial equivalent concentration profiles of Na and SO_4 as a function of distance after saturation with 0.5 M Na_2SO_4 solution. Dashed-dotted line and dashed-two dotted line indicate expected SO_4 and Na concentrations, respectively. These lines are estimated based on the assumption that the total porosity ($\varepsilon = 0.65$) is entirely filled with 0.5 M Na_2SO_4 solution.

assumption that total porosity was entirely filled with 0.5 M Na_2SO_4 solution. The total porosity ε was obtained as follows:

$$\varepsilon = 1 - \frac{\rho}{\rho_s} \tag{1}$$

where ρ is the dry density (1.0 kg/dm^3) and ρ_s is the solid grain density of the Kunipia F montmorillonite (2.88 kg/dm^3) (Sato et al., 1992; Tachi et al., 2014). The total porosity was estimated to be $\varepsilon = 0.65$. The experimentally determined Na and SO_4 concentrations were lower than the expected concentrations. This result has been explained by two contrasting models: anion exclusion (Van Loon et al., 2007) or Donnan equilibrium (Birgersson and Karnland, 2009). In this study, the widely used anion exclusion model was adopted. Three types of pores, interlayer, interparticle space and diffuse double layer, around the particle of the montmorillonite stacks, were considered. Assuming that the anions are completely excluded from the interlayer and diffuse double layer, the anions were considered to occur only in the interparticle space with the same concentration as the external solution (in this study, 0.5 M Na_2SO_4). In this case, the anion accessible porosity, ε_{acc}, can be obtained as follows:

$$\varepsilon_{acc} = \frac{C_{SO_4}}{z_{SO4}\,[SO_4]} \cdot \rho \tag{2}$$

where C_{SO4} is an averaged equivalent concentration of SO_4 per unit of dry montmorillonite determined as $C_{SO4} = 0.18$ eq/kg from the experiment as shown in Fig. 3, $[SO_4]$ is the molarity of SO_4 in the external solution ($[SO_4] = 0.5$ M), and z_{SO4} is the valence. In contrast, an averaged equivalent concentration of Na was determined as $C_{Na} = 1.27$ eq/kg from the experiment as shown in Fig. 3. It is necessary to satisfy an electro-neutrality condition anywhere in the montmorillonite as follows:

$$C_{Na} - CEC = C_{Na,free} = C_{SO4} \tag{3}$$

where $C_{Na,free}$ is the equivalent Na concentration in the interparticle space. The value of $C_{Na,free} = 0.22$ eq/kg was approximately consistent with $C_{SO4} = 0.18$ eq/kg. Therefore, the anion accessible porosity can be estimated to be $\varepsilon_{acc} = 0.20$, using the average values of $C_{Na,free} = 0.22$ eq/kg and $C_{SO4} = 0.18$ eq/kg.

3.2. Electromigration of $^{22}Na^+$, $^{45}Ca^{2+}$, $^{35}SO_4^{2-}$, and HTO

Fig. 4 shows the relative concentration profiles of $^{22}Na^+$, $^{45}Ca^{2+}$, $^{35}SO_4^{2-}$ and HTO obtained from the electromigration experiments as a function of distance from the initial position after applying 5 mA for 86,400 s. In the case of Na-montmorillonite saturated with 0.5 M Na_2SO_4 solution, the $^{35}SO_4^{2-}$ ions slightly migrated toward the anode (+), and the $^{22}Na^+$ ions and HTO migrated toward the cathode (−) under the electric potential gradient. At the same time, $^{22}Na^+$, $^{45}Ca^{2+}$, and HTO migrated to the cathode (−) in the Na/Ca-mixed

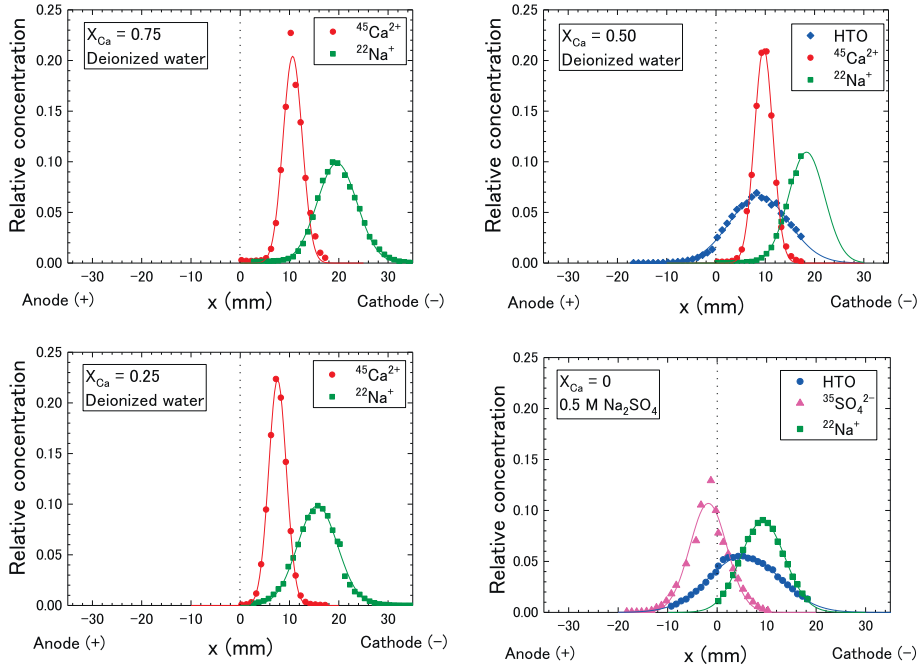

Fig. 4. Relative concentration profiles of $^{22}Na^+$, $^{45}Ca^{2+}$, $^{35}SO_4^{2-}$ ions and HTO using different X_{Ca} and solutions (deionized water or 0.5 M Na_2SO_4) as a function of the initial position after applying 5 mA for 86,400 s.

Table 1
Apparent migration velocity (V_a), hydrodynamic dispersion coefficient (D_h), transport number (t), electric potential gradient (E), apparent mobility (u_a), electromigration mobility (u_{em}), and apparent diffusion coefficient (D_a) of each species i obtained from electromigration experiments with different calcium equivalent fractions (X_{Ca}) and solutions (deionized water or 0.5 M Na_2SO_4).

X_{Ca}	Solution	Species i	$V_{a,i}$ [m/s]	$D_{h,i}$ [m^2/s]	t_i [−]	E [V/m]	$u_{a,i}$ [m^2/(s·V)]	$u_{em,i}$ ($=u_{a,i}-u_{a,HTO}$)	$D_{a,i}$ [m^2/s] (from $u_{a,i}$)	$D_{a,i}$ [m^2/s] (from $u_{em,i}$)	$D_{a,i}$ [m^2/s] (In-diffusion)
0 (X_{Na} = 1)	0.5 M Na_2SO_4	HTO	6.4×10^{-8}	2.9×10^{-10}	–	17	3.7×10^{-9}	–	–	–	–
		$^{35}SO_4^{2-}$	-2.0×10^{-8}	8.1×10^{-11}	0.02	17	-1.2×10^{-9}	-4.9×10^{-9}	1.5×10^{-11}	6.3×10^{-11}	9.5×10^{-11}
		$^{22}Na^+$	1.1×10^{-7}	1.2×10^{-10}	0.85	17	6.3×10^{-9}	2.5×10^{-9}	1.6×10^{-10}	6.5×10^{-11}	–
0.25	Deionized water	$^{45}Ca^{2+}$	8.8×10^{-8}	1.9×10^{-11}	0.14	66	1.3×10^{-9}	–	1.7×10^{-11}	–	1.6×10^{-11}[a]
		$^{22}Na^+$	1.8×10^{-7}	9.5×10^{-11}	0.86	66	2.7×10^{-9}	–	7.0×10^{-11}	–	7.1×10^{-11}[b]
0.50	Deionized water	HTO	1.0×10^{-7}	2.1×10^{-10}	–	90	1.1×10^{-9}	–	–	–	–
		$^{45}Ca^{2+}$	1.1×10^{-7}	2.0×10^{-11}	0.36	90	1.2×10^{-9}	1.2×10^{-10}	1.6×10^{-11}	1.5×10^{-12}	1.6×10^{-11}[a]
		$^{22}Na^+$	2.1×10^{-7}	7.7×10^{-11}	0.68	90	2.4×10^{-9}	1.2×10^{-9}	6.1×10^{-11}	3.2×10^{-11}	7.3×10^{-11}[b]
0.75	Deionized water	$^{45}Ca^{2+}$	1.2×10^{-7}	2.2×10^{-11}	0.59	82	1.5×10^{-9}	–	1.9×10^{-11}	–	1.5×10^{-11}[a]
		$^{22}Na^+$	2.3×10^{-7}	9.4×10^{-11}	0.36	82	2.8×10^{-9}	–	7.1×10^{-11}	–	7.1×10^{-11}[b]

[a] Kozaki et al. (2010).
[b] Kozaki et al. (2005).

montmorillonite saturated with deionized water. From the migration behaviors of $^{45}Ca^{2+}$ and $^{35}SO_4^{2-}$, it was expected that these species can be mixed with each other when a current is applied to the pair of Na/Ca-mixed montmorillonite and Na-montmorillonite saturated with 0.5 M Na_2SO_4 solution. The electromigration of chemical species can be described using the solution of a one-dimensional advection dispersion equation under the pulse input initial condition (Maes et al., 1999; Tanaka et al., 2011) as follows:

$$C_{r,i} = \frac{1}{2\sqrt{\pi D_{h,i} t}} \exp\left\{-\frac{(x - V_{a,i}t)^2}{4D_{h,i}t}\right\} \quad (4)$$

where $C_{r,i}$ is the relative concentration, $D_{h,i}$ is the hydrodynamic dispersion coefficient, and $V_{a,i}$ is the apparent migration velocity of species i. The $D_{h,i}$ and the $V_{a,i}$ were obtained from least-squares fits to Eq. (4). These values are summarized in Table 1. The $D_{h,i}$ can be expressed as the sum of the apparent diffusion coefficient $D_{a,i}$ and mechanical dispersion coefficient $D_{m,i}$ as follows:

$$D_{h,i} = D_{a,i} + D_{m,i} \quad (5)$$

$D_{h,i}$ was nearly equal to the $D_{a,i}$ from in-diffusion experiments for all species, suggesting that mechanical dispersion arising from advection is negligibly small in this study.

Assuming that all the Na, Ca, and SO_4 occur as mobile ions (Na^+, Ca^{2+}, and SO_4^{2-}) in the compacted montmorillonite, a transport number, t_i, which is the ratio of charge carried by each ion divided by the total current-carrying charge, can be obtained (Higashihara et al., 2008) as follows:

$$t_i = \frac{|V_{a,i}| \bullet S \bullet \rho \bullet C_i \bullet F}{I} \quad (6)$$

where S is the cross section of the montmorillonite specimen (3.14×10^{-4} m^2), ρ is the dry density (kg/dm^3), C_i is the equivalent concentration per unit of dry montmorillonite (eq/kg), F is the Faraday constant (9.65×10^4C/mol), and I is the current (A = C/s). The transport numbers of each ion are also summarized in Table 1. The transport number is basically proportional to the C_i and the $V_{a,i}$ of each ion. The transport number of the SO_4^{2-} ions was 0.02 in the case of the Na-montmorillonite saturated with 0.5 M Na_2SO_4 solution. This means that 2% of the charge was carried by SO_4^{2-} ions. The sum of the transport numbers of Na^+ and SO_4^{2-} ions was estimated to be 0.87. The underestimation of the transport numbers of Na^+ and SO_4^{2-} ions ($t_{Na} + t_{SO4} < 1$) may be because of the effect of the ion pair of $NaSO_4^-$ formed in the 0.5 M Na_2SO_4 solution. In contrast, the sum of the transport numbers of Na^+ and Ca^{2+} in the Na/Ca-mixed montmorillonite saturated with deionized water were nearly equal to 1 for all X_{Ca}, indicating that all of the Na and Ca were occurring as exchangeable cations (Na^+ and Ca^{2+}), and these ions can electrically migrate in the compacted Na/Ca-mixed montmorillonite.

The apparent migration velocities are proportional to the electric potential gradient, E, as follows:

$$V_{a,i} = u_{a,i}E \quad (7)$$

where $u_{a,i}$ is the apparent mobility. If the water as a migration medium moves, the relative velocity of the ions to the water velocity must be considered. An apparent electromigration mobility without the effect of water flow, u_{em}^i, can be obtained from a relation (Tanaka et al., 2011) as follows:

$$u_{em,i} = u_{a,i} - u_{a,HTO} \quad (8)$$

A relation between the mobilities u_i ($u_{a,i}$ or $u_{em,i}$) and the apparent diffusion coefficient, $D_{a,i}$, can be expressed by an Einstein relation (Atkins, 1998; Maes et al., 1999; Tanaka et al., 2011) as follows:

$$D_{a,i} = u_i \frac{kT}{z_i e} \quad (9)$$

where k is the Boltzmann constant, e is the elementary charge, and T is the absolute temperature.

As compared to D_a from the Einstein relation with D_a from the in-diffusion experiments shown in Table 1, the D_a of the cations obtained from $u_{a,i}$ (without water correction) are in good agreement with the D_a obtained from the in-diffusion experiment (Kozaki et al., 2005; Kozaki et al., 2010). On the other hand, the D_a of the SO_4^{2-} ions obtained from $u_{em,i}$ (with water correction) is roughly in agreement with the D_a obtained from in-diffusion experiment. These results are consistent with previous findings (Tanaka et al., 2011) that the effect of electro-osmotic water flow on electro-migrations of ions is greater for anions than for cations, suggesting that cations and anions migrate mainly in the interlayer and the interparticle space in the compacted montmorillonite (ρ = 1.0 kg/dm^3), respectively. These findings support the validity of assuming anion exclusion as previously mentioned in Section 3.1.

3.3. Gypsum precipitation after current application

Fig. 5 shows the equivalent concentration profiles of Na, Ca, and SO_4 after gypsum precipitation experiments using different initial X_{Ca} (0.10, 0.25, 0.50, and 0.75). The horizontal dashed lines correspond to the CEC of the montmorillonite (=1.05 eq/kg). The calcium concentration includes mobile chemical forms (exchangeable Ca^{2+} in the montmorillonite, free Ca^{2+}, and $CaSO_4^0$ as ion pairs in the interparticle space) and immobile $CaSO_4$ as precipitates. In the region < 0 mm, total calcium concentrations remained constant at the initial values. With increasing distance from 0 mm, calcium concentrations drastically increased except for the case of X_{Ca} = 0.10, and then gradually decreased to nearly zero. Mobile sodium concentrations including exchangeable

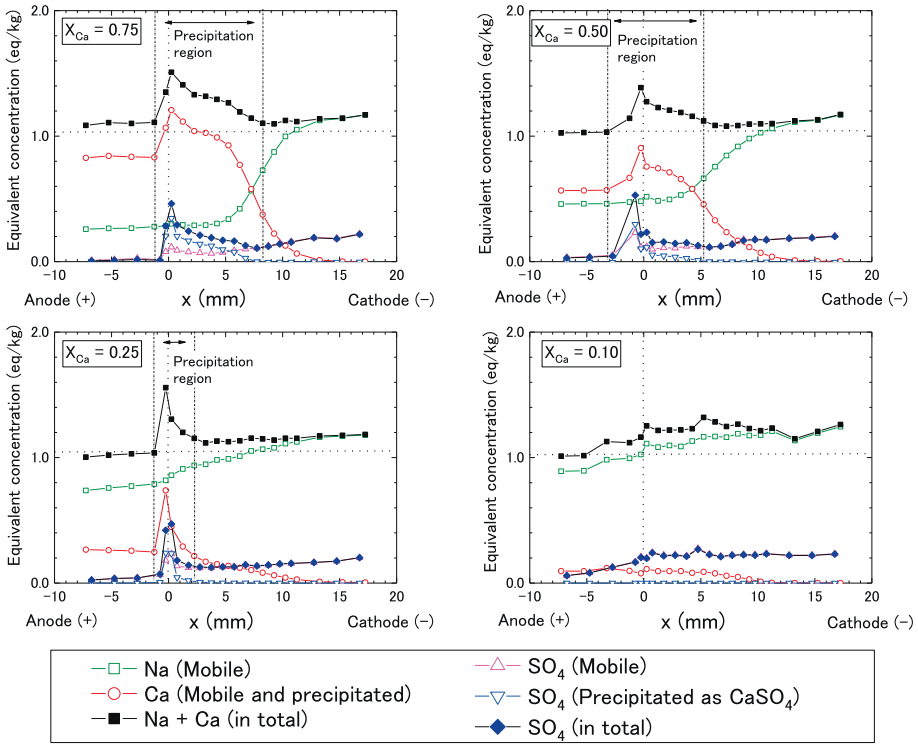

Fig. 5. Equivalent concentration profiles of Na, Ca, mobile SO_4, and precipitated SO_4 as a function of distance from the contact surface obtained from gypsum precipitation experiments (5 mA for 86,400 s) with different X_{Ca}.

Na^+ in the montmorillonite, free Na^+, and $NaSO_4^-$ as ion pairs also remained constant in the region < 0 mm and increased with increasing distance. Focusing on the precipitated SO_4 concentrations, the peaks emerged in the same region as that of Ca peaks at X_{Ca} = 0.25, 0.50, and 0.75, and no peak was observed at X_{Ca} = 0.10. Therefore, the significant concentration peaks of Ca and SO_4 are considered to be derived from $CaSO_4$ precipitation. The precipitation front shifted to the cathode side with increasing X_{Ca}, because the V_a of SO_4^{2-} ions was approximately one-fifth of those of Ca^{2+} as listed in Table 1. In the case of X_{Ca} = 0.75, the precipitation region was 9.5 mm in length, while in the case of X_{Ca} = 0.25, the region was 3.5 mm in length as shown in Fig. 5. The length of the regions may be associated with the extent of supersaturation of the solution (discussed in Section 3.5). The mobile SO_4 concentrations gradually increased with increasing distance, and finally correspond to the trend of Na concentrations greater than the CEC value. The total Na and Ca concentrations greater than the CEC value showed a similar trend to that of total SO_4 concentrations for all positions, suggesting that electrical neutrality and material balance are satisfied in the experiments.

3.4. Gypsum crystal aggregation examined using XRD and EPMA

Fig. 6 shows the XRD patterns of the montmorillonite powders at different distances from the contact surface after the precipitation experiment at X_{Ca} = 0.75. The XRD data of gypsum ($CaSO_4 2H_2O$) was obtained from the inorganic material database "AtomWork" (Xu et al., 2011). Peaks for gypsum were observed up to 7.5–8.5 mm, and the height of the peaks decreased with increasing distance from the contact surface. These results are consistent with the concentration of precipitated $CaSO_4$ which decreased with increasing distance at X_{Ca} = 0.75 (Fig. 5). The XRD patterns indicate that $CaSO_4$ precipitated, at least in part, as gypsum in the montmorillonite.

Fig. 7 shows BSE images and elemental maps obtained using EPMA near the contact surface (0.0–1.0 mm) perpendicular to the *x* direction, following the gypsum precipitation experiment at X_{Ca} = 0.75. BSE

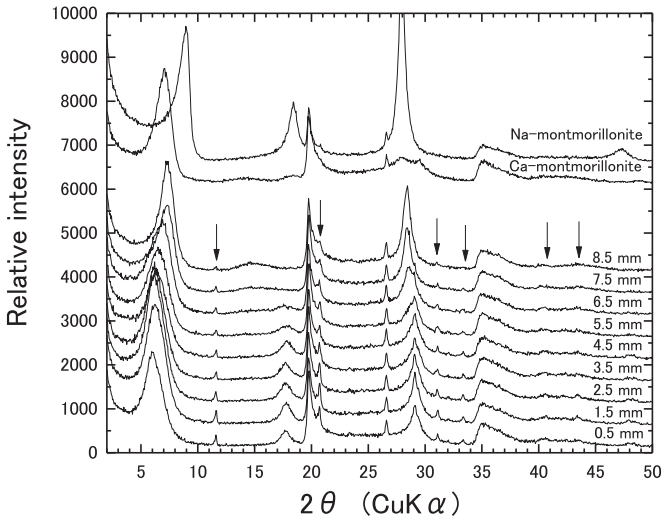

Fig. 6. X-ray diffraction patterns as a function of distance from the contact surface after applying 5 mA for 86,400 s (X_{Ca} = 0.75) with those of Na- and Ca-montmorillonite. Arrows indicate peaks from gypsum ($CaSO_4 2H_2O$).

images reflect different chemical compositions. In the overall view (a), the white spots observed in the BSE image were in good agreement with Ca and S in the elemental maps, suggesting that gypsum precipitates in these areas. In contrast, the Si, Al, and Mg derived from the montmorillonite structure were absent in the spots. Aggregations were also observed in the 6.0–7.0 mm slices (not shown), but more sparsely precipitated and of similar size. It is known that nuclei that are larger than the critical size grow without limit, whereas those that are smaller dissolve again (Gebauer and Cölfen, 2011), resulting in the formation of sparsely precipitated aggregates. From the magnified images of a single aggregate (b), a large aggregate approximately 300 μm infiltrated into the montmorillonite texture. The observed fractal-like growth of the

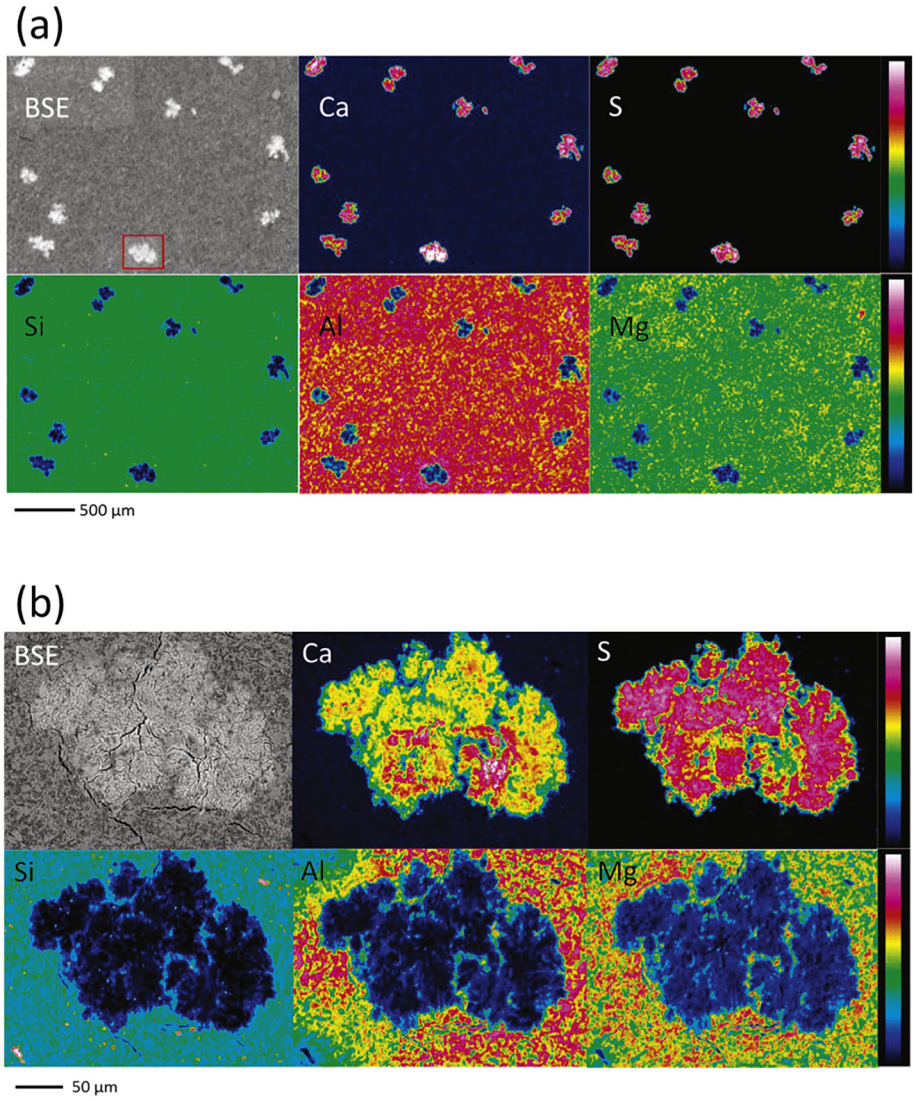

Fig. 7. Back scattered electron (BSE) images and elemental maps of the precipitates observed by electron probe X-ray microanalysis (EPMA). (a) Overall view, (b) a single aggregate at the area of red square in the image (a).

aggregates may be because of diffusional transport of Ca^{2+} and SO_4^{2-} ions perpendicular to the x direction in the montmorillonite, termed diffusion limited aggregation (Witten and Sander, 1981). During this process, a seed crystal grows into a highly branched and fractal structure by sticking randomly moving ions as raw materials. The basic concept is explained by Halsey (2000). From the results of the electromigration experiment (Fig. 4), the average migration distance of species i because of advection to the x direction, $L_{V,i}$, at a given time can be estimated as follows:

$$L_{V,i} = V_{a,i}t \tag{10}$$

The root mean square distance due to the hydrodynamic dispersion, $L_{D,i}$, which is a measure of the spread of species i (Atkins, 1998) can be obtained as follows:

$$L_{D,i} = \sqrt{2D_{h,i}t} \tag{11}$$

The estimated distances, $L_{V,i}$ and $L_{D,i}$, of Ca and SO_4 at 86,400 s with different X_{Ca} are listed in Table 2. The $L_{V,Ca}$ values, because of advection, were 4–5 times greater than those of $L_{D,Ca}$, because of the dispersion. The $L_{V,SO4}$ was a negative value and of similar extent to $L_{D,SO4}$. Mechanical dispersion was negligibly small as previously mentioned in Section 3.2, therefore, the mass transport perpendicular to the x direction was similar to the diffusional transport for all species. The difference between $L_{V,i}$ and $L_{D,i}$ indicates that the mixing of Ca and SO_4 was dominated by advective transport into the x direction; however, it is likely that the diffusional transport of Ca and SO_4 in all directions resulted in fractal-like gypsum aggregations, which were sparsely precipitated in the compacted montmorillonite.

3.5. Porewater chemistry of gypsum precipitation

In the results of the precipitation experiments as shown in Fig. 5, gypsum peaks were observed at X_{Ca} = 0.25, 0.50 and 0.75. There was no peak when the ionic equivalent fraction of calcium in the montmorillonite decreased to X_{Ca} = 0.10. These results suggest that the threshold X_{Ca} for gypsum precipitation is between X_{Ca} = 0.10 and X_{Ca} = 0.25 under the experimental conditions (a dry density of 1.0 kg/dm^3 saturated with 0.5 M Na_2SO_4 solution). To discuss in detail the gypsum precipitation and porewater chemistry in compacted montmorillonite, chemical speciation calculations of Na, Ca, and SO_4 for the montmorillonite specimens following electrical current application were conducted using the PHREEQC code (Ver.2.18). In the calculation, it is necessary to specify concept regarding the microstructure and ion distribution in the compacted montmorillonite. However, no commonly

Table 2
Average migration distances due to advection, $L_{V,b}$ and the root mean square distances due to dispersion, $L_{D,b}$ of Ca^{2+} and SO_4^{2-} ions estimated from $V_{a,i}$ and $D_{h,i}$ with different equivalent calcium fractions (X_{Ca}) at 86,400 s.

Species i	Solution	X_{Ca}	$V_{a,i}$ [m/s]	$D_{h,i}$ [m^2/s]	$L_{V,i}$ [m]	$L_{D,i}$ [m]
SO_4^{2-}	0.5 M Na_2SO_4	0	-2.0×10^{-8}	8.1×10^{-11}	-1.7×10^{-3}	3.7×10^{-3}
Ca^{2+}	Deionized water	0.25	8.8×10^{-8}	1.9×10^{-11}	7.6×10^{-3}	1.8×10^{-3}
		0.50	1.1×10^{-7}	2.0×10^{-11}	9.5×10^{-3}	1.9×10^{-3}
		0.75	1.2×10^{-7}	2.2×10^{-11}	1.0×10^{-2}	2.0×10^{-3}

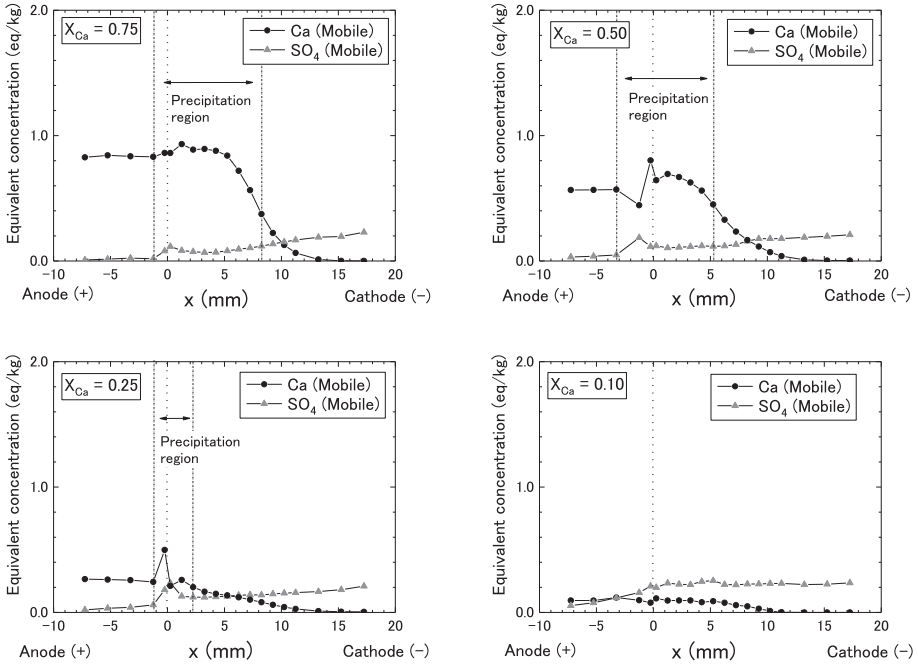

Fig. 8. Equivalent concentration profiles of mobile Ca and SO_4 as a function of distance from the contact surface with different X_{Ca}. The mobile Ca and SO_4 concentrations were obtained from deducting immobile (precipitated) $CaSO_4$ concentration from the total Ca and SO_4 concentrations shown in Fig. 5.

established model is available for this problem. In this discussion, anions are assumed to be completely excluded from the interlayer and diffuse double layer in the compacted montmorillonite, and only occurring in the interparticle solution. Then, the experimentally estimated anion accessible porosity $\varepsilon_{acc} = 0.20$ in the Na-montmorillonite saturated with 0.5 M Na_2SO_4 solution (Fig. 3) was used in the calculation. Because the molarity of the Na_2SO_4 solution is quite high, up to 0.5 M, the value of the anion accessible porosity was assumed to be unchanged in the calculation. Detailed procedures are described in the following paragraphs.

Fig. 8 shows the mobile Ca and SO_4 concentrations obtained from deducting precipitated $CaSO_4$ from the total Ca and SO_4 concentrations shown in Fig. 5. Although disturbance of calcium concentrations near the contact surface ($x = 0$ mm) were observed particularly at $X_{Ca} = 0.25$ and 0.50, the mobile Ca concentrations maintained their initial value until the contact surface, and gradually decreased with increasing distance. The mobile SO_4 concentrations increased with increasing distance and approached the initial value (0.20 eq/kg). The mobile Ca was considered to have occurred as exchangeable Ca^{2+} in the montmorillonite, free Ca^{2+} ions, and $CaSO_4^0$ as ion pairs in the interparticle solution. In the PHREEQC calculation, it was assumed that all the Ca was initially occurring as exchangeable cations in the montmorillonite. Exchangeable cations in the montmorillonite are composed of Na^+ and Ca^{2+} ions in this study; therefore, the sum of the ionic equivalent fractions of cation is equal to 1 ($X_{Na} + X_{Ca} = 1$). Thus, the initial X_{Ca} and X_{Na} can be estimated as follows:

$$X_{Ca} = \frac{C_{Ca}}{CEC} \tag{12}$$

$$X_{Na} = 1 - X_{Ca} \tag{13}$$

where C_{Ca} is the experimentally determined mobile Ca equivalent concentration per unit of dry montmorillonite as shown in Fig. 8. In contrast, the mobile SO_4 is considered to occur as free SO_4^{2-} ions and ion pairs of $NaSO_4^-$ and $CaSO_4^0$ in the interparticle solution. Similarly, the Na in the interparticle solution are considered to occur as free Na^+ ions and ion pairs of $NaSO_4^-$ ions. In the PHREEQC calculation, it was assumed that all the SO_4 was occurring in the interparticle solution; therefore the molarity of the mobile SO_4 can be estimated as follows:

$$[SO_4] = \frac{C_{SO4}\rho}{z_{SO4}\varepsilon_{acc}} \tag{14}$$

where C_{SO4} is the experimentally determined mobile SO_4 equivalent concentration per unit of dry montmorillonite (eq/kg) as shown in Fig. 8. The other values were $\rho = 1.0$ kg/dm^3, $z_{SO4} = 2$, and $\varepsilon_{acc} = 0.20$. The Na concentration in the interparticle solution, [Na], was estimated from [SO_4] to be satisfied with the electrical neutrality,

$$[Na] = 2[SO_4] \tag{15}$$

The estimated initial X_{Ca} and X_{Na}, and initial molarities of [SO_4] and [Na], were used as input values for the PHREEQC speciation calculation. Note that the initial distribution of species between the montmorillonite and the interparticle solution does not affect the final result of the equilibrated speciation if the mass of each Na, Ca and SO_4 are fixed in the entire system.

A cation exchange reaction is generally explained by a concept of a selectivity coefficient. The exchange reaction between Na^+ and Ca^{2+} in the montmorillonite can be written as follows:

$$2NaX + Ca^{2+} \Leftrightarrow 2Na^+ + CaX_2 \quad (16)$$

The Gaines-Thomas selectivity coefficient (Gaines and Thomas, 1953), K_{GT}, for the reaction of Eq. (16) was adopted in the calculation. The coefficient can be written as follows:

$$K_{GT} = \frac{X_{Ca} \bullet a_{Na^+}^2}{(1 - X_{Ca})^2 \bullet a_{Ca^{2+}}} \quad (17)$$

where a is the activity of each ion in the interparticle solution. Eq. (17) indicates that X_{Ca} is the only variable affecting a_{Ca} when K_{GT} and a_{Na} are fixed. In the case that the Na_2SO_4 concentration changes, however, not only a_{SO4} but also a_{Na} change, resulting in a change of a_{Ca} as indicated by Eq. (17). This reaffirms a feature that X_{Ca} is suitable for a variable to investigate the gypsum precipitation reaction rather than Na_2SO_4 concentration, as mentioned in the introduction.

The formation of $CaSO_4^0$ and $NaSO_4^-$ can be written as follows:

$$Ca^{2+} + SO_4^{2-} \Leftrightarrow CaSO_4^0 \quad (18)$$

$$Na^+ + SO_4^{2-} \Leftrightarrow NaSO_4^- \quad (19)$$

and the equilibrium constants can be written as

$$K_{Ca} = \frac{a_{CaSO_4^0}}{a_{Ca^{2+}} \bullet a_{SO_4^{2-}}} \quad (20)$$

$$K_{Na} = \frac{a_{NaSO_4^-}}{a_{Na^+} \bullet a_{SO_4^{2-}}} \quad (21)$$

where K_{Ca} and K_{Na} are the stability constants for each ion pair. The gypsum precipitation and dissolution reaction is as follows:

$$CaSO_4 \cdot 2H_2O \Leftrightarrow Ca^{2+} + SO_4^{2-} + 2H_2O \quad (22)$$

The ion activity product (*IAP*) for Eq. (22) can be expressed as follows:

$$IAP = a_{Ca^{2+}} \cdot a_{SO4^{2-}} \cdot a_{H_2O}^2 = [Ca^{2+}]\gamma_{Ca^{2+}}[SO_4^{2-}]\gamma_{SO_4^{2-}} \cdot a_{H_2O}^2 \quad (23)$$

where $[Ca^{2+}]$ and $[SO_4^{2-}]$ are the molarities of the free Ca^{2+} and SO_4^{2-} in the interparticle solution, and γ_{SO4} and γ_{Ca} are the activity coefficients of each ion, respectively. The activity coefficients of ions were calculated from the WATEQ Debye-Hückel or Davies equation based on the database in PHREEQC Ver.2.18 (Parkhurst and Appelo, 1999).

The speciation calculations were conducted using the "MIX" function with a solid/liquid ratio of 1/0.2 = 5 kg/dm^3, which was derived from the dry density of 1.0 kg/dm^3 and $\varepsilon_{acc} = 0.20$. The equilibrated concentrations of each chemical species (X_{Ca}, X_{Na}, $[Ca^{2+}]$, $[SO_4^{2-}]$, $[Na^+]$, $[NaSO_4^-]$, and $[CaSO_4^0]$) were calculated at each point shown in Fig. 8. Then, saturation indices (SIs) were obtained as follows:

$$SI = \log\left(\frac{IAP}{K_{sp}}\right) \quad (24)$$

where K_{sp} is the solubility product of the gypsum under ambient conditions. All the equilibrium constants used in the calculation are listed in Table 3. Note that the maximum volume of the precipitated gypsum, which corresponds to the position around the contact surface of $X_{Ca} = 0.25$ shown in Fig. 5, accounts for approximately 10% of the anion accessible porosity of $\varepsilon_{acc} = 0.20$. This value is of similar extent to the error in the ε_{acc} estimation. Therefore, the effect of gypsum precipitation (clogging) on the PHREEQC calculation was considered to be negligibly small.

Fig. 9 shows SIs at different K_{GT} values for the results of the precipitation experiments (Fig. 5). An SI > 0 implies that the solution is supersaturated with respect to gypsum, and the solutes have a tendency to precipitate as gypsum. In the case of $K_{GT} = 4.9$ (corresponding to $\log K_{GT} = 0.69$), which was already reported from the batch experiment at a solid/liquid ratio of 0.01 kg/dm^3 under the Kunipia-F montmorillonite (Oda and Shibata, 1999), the regions where the SI was > 0 were much more widespread than the experimentally determined precipitation regions. In the case that the value was assumed to be $K_{GT} = 200$, the regions where SI was > 0 were in good agreement with the experimentally determined precipitation regions at $X_{Ca} = 0.25$, 0.50, and 0.75 as shown in Fig. 9, and the SI < 0 over the entire region at $X_{Ca} = 0.10$.

Table 3
Equilibrium constants used in the calculation to estimate saturation indices of gypsum.

Reactions	log K
Solubility product of gypsum $CaSO_4 \cdot 2H_2O \Leftrightarrow Ca^{2+} + SO_4^{2-} + 2H_2O$	−4.58[a]
Ion exchange between Na^+ and Ca^{2+} $2NaX + Ca^{2+} \Leftrightarrow 2Na^+ + CaX_2$ (Gains-Thomas convention)	0.69[b] ($K_{GT} = 4.9$)
Stability constant $Ca^{2+} + SO_4^{2-} \Leftrightarrow CaSO_4^0$ $Na^+ + SO_4^{2-} \Leftrightarrow NaSO_4^-$	 2.3[a] 0.7[a]

[a] Default values of PHREEQC database file.
[b] Reported value from batch experiment using Kunipia-F montmorillonite (Oda and Shibata, 1999)

It is known that the solubility of a crystal increase in a confined state than in an unconfined state. Detailed discussion regarding nucleation and crystal growth are beyond the scope of this paper; however, the effects of pore size and swelling pressure on the solubility product of gypsum in terms of thermodynamics are discussed. Crystal growth in porous materials under a confined state is explained in detail (Steiger, 2005a, 2005b). Based on these research studies, the extent of solubility deviation (SD) from ambient conditions can be defined as follows:

$$SD = \log\left(\frac{K_{sp}^*}{K_{sp}}\right) = \frac{V_m}{2.3RT}\left(\Delta p + \frac{2\overline{\gamma}_{cl}}{r}\right) \quad (25)$$

where r is the radius of a small spherical particle, Δp is the swelling pressure, K_{sp}^* is the solubility product of gypsum under a confined state, $\overline{\gamma}_{cl} = 6.5 \times 10^{-2}$ N/m is the mean surface free energy, and $V_m = 7.4 \times 10^{-5}$ m^3/mol is the molar volume of gypsum (Serafeimidis and Anagnostou, 2014). Although Eq. (25) may be used in a spherical crystal in a spherical pore (Steiger, 2005b), the equation provide a valuable insight into the gypsum supersaturation under a confined state. When assuming a radius of $r = 8 \times 10^{-9}$ m, which is one half of the maximum average pore spacing of the Na-montmorillonite at a dry density of 1.0 kg/dm^3 saturated with deionized water (Kozaki et al., 2001), and a swelling pressure $\Delta p = 1 \times 10^6$ N/m^2 at a dry density of 1.0 kg/dm^3 as summarized by Sato (2008), the extent of SD can be estimated as SD = 0.22. If only the effect of Δp is considered, which corresponds to a large crystal ($r = \infty$), the SD is 0.01, indicating that the supersaturation required for the growth of a large gypsum aggregate ($r = \infty$) is not significant even under a swelling pressure of 10^6 N/m^2 ($\rho = 1.0$ kg/dm^3). The maximum pore space in this study would be greater than that reported by Kozaki et al. (2001) because the solution used in this study was 0.5 M Na_2SO_4 solution in place of deionized water. The high salt concentration facilitates montmorillonite aggregation, and the nucleation tends to occur in larger pore space than average pore space. Therefore, the extent of solubility deviation of gypsum under a confined state in this study can be considered as SD < 0.22. This means that the much more widespread supersaturation regions (SI > 0) when using $K_{GT} = 4.9$ (reported from the batch experiment) as shown in Fig. 9 are not because of the effect of the greater solubility product of gypsum under a confined state, but may be because of the K_{GT} deviation ($K_{GT} = 200$) in a confined state. When

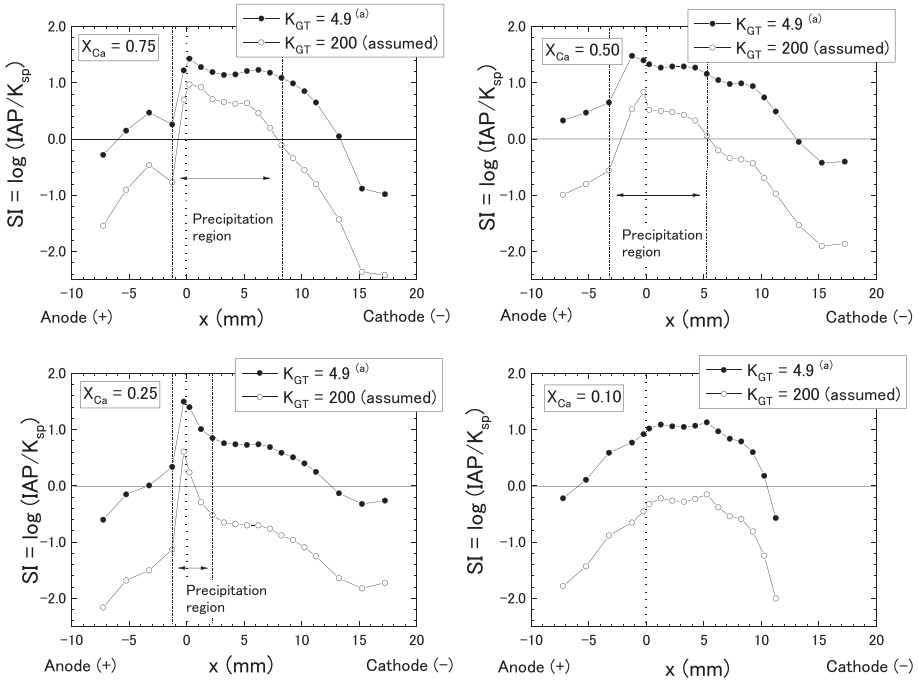

Fig. 9. Saturation indices (SIs) following precipitation experiments as a function of distance from the contact surface with different K_{GT} values calculated by the PHREEQC code. (d) Oda and Shibata (1999).

considering the case of $r = 5 \times 10^{-10}$ m, which corresponds to one half of the interlayer distance of three-water-layer hydrate (Kozaki et al., 1998), the SD is 3.4, which means that K_{sp}^{*} is three orders of magnitude greater than K_{sp}. This indicates that gypsum precipitation is unlikely in the interlayer space.

The result showing that the precipitation front shifted to the cathode side with increasing X_{Ca}, and the significant peak observed at $X_{Ca} = 0.25$ around the contact surface as shown in Fig. 5, may be because of a difference in the supersaturation required between nucleation and crystal growth. When the supersaturation is much greater than the value required for nucleation in the pore space, it is possible that both nucleation and crystal growth occur simultaneously in the small pore space. This may correspond to $X_{Ca} = 0.75$ in this study. In contrast, in the case that the supersaturation is initially greater than the value required for the nucleation around the contact surface, but the supersaturation quickly decreases to value less than that required for nucleation, the nuclei initially generated around the contact surface will preferentially grow. This may correspond to $X_{Ca} = 0.25$ in this study.

The extent of the supersaturation as shown in Fig. 9 (at $K_{GT} = 200$) in the precipitation regions is much > 0 although large gypsum aggregates are occurring around the regions. This suggests that the regions are far from the gypsum precipitation equilibrium. This result may be due to the slow mass transport of the Ca^{2+} and SO_4^{2-} ions in all directions in the montmorillonite as discussed in Section 3.4. In the EPMA observations as shown in Fig. 7, the distances among the gypsum aggregates were up to approximately 1–2 mm, which are comparable to the average migration distances of Ca^{2+} and SO_4^{2-} because of the dispersion ($L_{D,i}$) as shown in Table 2. It is likely that the randomly moving Ca^{2+} and SO_4^{2-} ions that escaped incorporation into the growing crystals contribute to the SI > 0 around the precipitation regions.

It is likely that the overestimation of the SI is because of overestimated free Ca^{2+} concentrations in the interparticle solution when using $K_{GT} = 4.9$ from the dispersed experiments. The tendency that K_{GT} slightly increases in a highly compacted state compared to loosely compacted or dispersed states was reported using Poisson-Boltzmann theory ($K_{GT} = 8$–8.1 at a dry density of 1.7 kg/dm^3, and $K_{GT} = 5.1$–5.3 at a dry density of 1.35 kg/dm^3) (Hedström and Karnland, 2011). In addition, it has been reported that the experimentally determined K_{GT} between the external solution and the compacted montmorillonite does not show a clear density correlation ($K_{GT} = 3.8$–7.8) and is similar to those reported for a dispersed state (Karnland et al., 2011). The K_{GT} obtained from the external activities of Na^+ and Ca^{2+} (Karnland et al., 2011) was considered to correspond to the K_{GT} defined by the interparticle activity under the anion exclusion assumption in this study. However, the $K_{GT} = 200$ implied in this study is much greater than the reported values.

The much greater K_{GT} implied in this study is likely because of a difference between the internal and external solution in the compacted montmorillonite. In the PHREEQC calculation, it was assumed that anions are completely excluded from the interlayer and diffuse double layer around the montmorillonite stacks. In this case, the interparticle solution is free from the electrical charge of the montmorillonite sheets and has a similar composition to that of the external solution. In contrast, in the case that the effect of the electrical double layer is considered, the concentrations of the Ca^{2+} and SO_4^{2-} ions change with distance from the montmorillonite sheets. In accordance with this change, the activity coefficients of Ca^{2+} and SO_4^{2-} ions also change, and coupled with the effect of the charge from the montmorillonite. This results in complex activity distribution of Ca^{2+} and SO_4^{2-} ions in the interparticle solution. It is quite difficult to solve the problem of the gypsum precipitation reaction in this situation. As the fundamental problem, a framework of the selectivity coefficient is premised on the existence of free solution, in which the charge of the montmorillonite does not affect the composition of the solution and the activity coefficients of ion. The concept of a selectivity coefficient in Eq. (17) is likely to be applicable when assuming anion exclusion and the existence of free solution in the compacted bentonite. The much greater K_{GT} implied in this study may be attributed to neglecting the effect of the diffuse double layer around the montmorillonite stacks in the calculation. Although theoretical evidence of a greater K_{GT} remains a problem to be solved, the precipitation tendency of gypsum in this study may be explained by a model including anion exclusion and cation exchange

between the montmorillonite and interparticle solution when an adequate K_{GT} value is used in the calculation.

4. Conclusions

Porewater chemistry and calcium reactivity in compacted Na/Ca-mixed montmorillonite were investigated from a gypsum precipitation reaction enhanced by an electrokinetic method. From the electromigration experiments, the sum of the transport numbers of Na^+ and Ca^{2+} in the Na/Ca-mixed montmorillonite saturated with deionized water were nearly equal to 1 in all of the X_{Ca} conditions, indicating that all of the Na^+ and Ca^{2+} ions as exchangeable cations could electrically migrate. Gypsum precipitation was successfully enhanced by applying an electric current of 5 mA for 86,400 s. The results showed that $CaSO_4$ was sparsely precipitated as gypsum aggregates up to 300 μm as seen under XRD and EPMA observations, and the aggregates were growing into the montmorillonite texture. The threshold X_{Ca} for gypsum precipitation was experimentally found to be between $X_{Ca} = 0.1$ and $X_{Ca} = 0.25$ at a dry density of 1.0 kg/dm^3 saturated with 0.5 M Na_2SO_4 solution. SIs of gypsum following the precipitation experiments were evaluated based on a model including anion exclusion and cation exchange (Gains-Thomas selectivity coefficients, K_{GT}) between the montmorillonite and interparticle solution, with the assistance of the PHREEQC code. The gypsum precipitation regions were in good agreement with regions where the SI was greater than zero when assuming $K_{GT} = 200$, which is much greater than the $K_{GT} = 4.9$ reported from the batch experiment. The greater K_{GT} value implied in this study reflects a significant difference between the internal and external solution of the compacted montmorillonite. The reason for the K_{GT} deviation remains to be solved; however, the precipitation tendency of gypsum may be explained by a model including anion exclusion and cation exchange between the montmorillonite and interparticle solution when an adequate K_{GT} value is used in the calculation.

Acknowledgements

This work was supported by JSPS KAKENHI Grant Number 17K14906. The experiments using radioactive tracer were performed at the Central Institute of Isotope Science, Hokkaido University. The analysis of gypsum precipitated montmorillonite was carried out with EPMA at the “Joint-use Facilities: Laboratory of Nano-Micro Material Analysis”, Hokkaido University, supported by “Material Analysis and Structure Analysis Open Unit (MASAOU)”. Powder X-ray diffraction experiments were carried out using Cu- Kα radiation by a RINT-2000 diffractometer installed at MASAOU of Hokkaido University.

References

Alt-Epping, P., Tournassat, C., Rasouli, P., Steefel, C.I., Mayer, K.U., Jenni, A., Mäder, U., Sengor, S.S., Fernández, R., 2014. Benchmark reactive transport simulations of a column experiment in compacted bentonite with multispecies diffusion and explicit treatment of electrostatic effects. Comput. Geosci. 19, 535–550.

Alt-Epping, P., Gimmi, T., Wersin, P., Jenni, A., 2018. Incorporating electrical double layers into reactive-transport simulations of processes in clays by using the Nernst-Planck equation: a benchmark revisited. Appl. Geochem. 89, 1–10.

Atkins, P.W., 1998. Physical Chemistry Sixth Edition. Oxford University Press.

Beauwens, T., De Cannière, P., Moors, H., Wang, L., Maes, N., 2005. Studying the migration behaviour of selenate in Boom Clay by electromigration. Eng. Geol. 77, 285–293.

Bildstein, O., Trotignon, L., Perronnet, M., Jullien, M., 2006. Modelling iron–clay interactions in deep geological disposal conditions. Phys. Chem. Earth Parts A/B/C 31, 618–625.

Birgersson, M., 2017. A general framework for ion equilibrium calculations in compacted bentonite. Geochim. Cosmochim. Acta 200, 186–200.

Birgersson, M., Karnland, O., 2009. Ion equilibrium between montmorillonite interlayer space and an external solution—consequences for diffusional transport. Geochim. Cosmochim. Acta 73, 1908–1923.

Bourg, I.C., Sposito, G., Bourg, A.C.M., 2008. Modeling the diffusion of Na+ in compacted water-saturated Na-bentonite as a function of pore water ionic strength. Appl. Geochem. 23, 3635–3641.

De Windt, L., Marsal, F., Tinseau, E., Pellegrini, D., 2008. Reactive transport modeling of geochemical interactions at a concrete/argillite interface, Tournemire site (France). Phys. Chem. Earth Parts A/B/C 33, S295–S305.

Gaboreau, S., Prêt, D., Tinseau, E., Claret, F., Pellegrini, D., Stammose, D., 2011. 15 years of in situ cement–argillite interaction from Tournemire URL: characterisation of the multi-scale spatial heterogeneities of pore space evolution. Appl. Geochem. 26, 2159–2171.

Gaines, G.L., Thomas, H.C., 1953. Adsorption studies on clay minerals. II. A formulation of the thermodynamics of exchange adsorption. J. Chem. Phys. 21, 714–718.

Gaucher, E.C., Blanc, P., 2006. Cement/clay interactions—a review: experiments, natural analogues, and modeling. Waste Manag. 26, 776–788.

Gaucher, E.C., Tournassat, C., Pearson, F.J., Blanc, P., Crouzet, C., Lerouge, C., Altmann, S., 2009. A robust model for pore-water chemistry of clayrock. Geochim. Cosmochim. Acta 73, 6470–6487.

Gebauer, D., Cölfen, H., 2011. Prenucleation clusters and non-classical nucleation. Nano Today 6, 564–584.

Glaus, M.A., Baeyens, B., Bradbury, M.H., Jakob, A., Van Loon, L.R., Yaroshchuk, A., 2007. Diffusion of Na-22 and Sr-85 in montmorillonite: evidence of interlayer diffusion being the dominant pathway at high compaction. Environ. Sci. Technol. 41, 478–485.

Glaus, M.A., Frick, S., Rossé, R., Loon, L.R.V., 2010. Comparative study of tracer diffusion of HTO, 22Na+ and 36Cl− in compacted kaolinite, illite and montmorillonite. Geochim. Cosmochim. Acta 74, 1999–2010.

Halsey, T.C., 2000. Diffusion-limited aggregation: a model for pattern formation. Phys. Today 53, 36–41.

Hedström, M., Karnland, O., 2011. Ca/Na selectivity coefficients from the Poisson–Boltzmann theory. Phys. Chem. Earth Parts A/B/C 36, 1559–1563.

Higashihara, T., Kinoshita, K., Akagi, Y., Sato, S., Kozaki, T., 2008. Transport number of sodium ions in water-saturated, compacted Na-montmorillonite. Phys. Chem. Earth Parts A/B/C 33, S142–S148.

Karnland, O., 2010. Chemical and Mineralogical Characterization of the Bentonite Buffer for the Acceptance Control Procedure in a KBS-3 Repository. SKB Technical Report TR-10-60, SKB, Stockholm.

Karnland, O., Birgersson, M., Hedström, M., 2011. Selectivity coefficient for Ca/Na ion exchange in highly compacted bentonite. Phys. Chem. Earth Parts A/B/C 36, 1554–1558.

Kozaki, T., Fujishima, A., Sato, S., Ohashi, H., 1998. Self-diffusion of sodium ions in compacted sodium montmorillonite. Nucl. Technol. 121, 63–69.

Kozaki, T., Sato, H., Sato, S., Ohashi, H., 1999. Diffusion mechanism of cesium ions in compacted montmorillonite. Eng. Geol. 54, 223–230.

Kozaki, T., Inada, K., Sato, S., Ohashi, H., 2001. Diffusion mechanism of chloride ions in sodium montmorillonite. J. Contam. Hydrol. 47, 159–170.

Kozaki, T., Fujishima, A., Saito, N., Sato, S., Ohashi, H., 2005. Effects of dry density and exchangeable cations on the diffusion process of sodium ions in compacted montmorillonite. Eng. Geol. 81, 246–254.

Kozaki, T., Sawaguchi, T., Fujishima, A., Sato, S., 2010. Effect of exchangeable cations on apparent diffusion of Ca2+ ions in Na- and Ca-montmorillonite mixtures. Phys. Chem. Earth Parts A/B/C 35, 254–258.

Leroy, P., Revil, A., Coelho, D., 2006. Diffusion of ionic species in bentonite. J. Colloid Interface Sci. 296, 248–255.

Maes, N., Moors, H., Dierckx, A., Canniere, P.D., Put, M., 1999. The assessment of electromigration as a new technique to study diffusion of radionuclides in clayey soils. J. Contam. Hydrol. 36, 231–247.

Melkior, T., Mourzagh, D., Yahiaoui, S., Thoby, D., Alberto, J.C., Brouard, C., Michau, N., 2004. Diffusion of an alkaline fluid through clayey barriers and its effect on the diffusion properties of some chemical species. Appl. Clay Sci. 26, 99–107.

Melkior, T., Gaucher, E.C., Brouard, C., Yahiaoui, S., Thoby, D., Clinard, C., Ferrage, E., Guyonnet, D., Tournassat, C., Coelho, D., 2009. Na+ and HTO diffusion in compacted bentonite: effect of surface chemistry and related texture. J. Hydrol. 370, 9–20.

Muurinen, A., Karnland, O., Lehikoinen, J., 2004. Ion concentration caused by an external solution into the porewater of compacted bentonite. Phys. Chem. Earth Parts A/B/C 29, 119–127.

Oda, C., Shibata, M., 1999. Modeling and experimental studies on bentonite-water interaction [in Japanese]. In: JNC Technical Report, JNC TN8400, (Report No. 99–132).

Parkhurst, D.L., Appelo, C.A.J., 1999. User's Guide to PHREEQC (Version 2)-a Computer Program for Speciation, Batch-Reaction, one Dimensional Transport, and Inverse Geochemical Calculations. In: Water-Resources Investigations Report, (Report No. 99-4259).

Sato, H., 2008. Thermodynamic model on swelling of bentonite buffer and backfill materials. Phys. Chem. Earth Parts A/B/C 33, S538–S543.

Sato, H., Ashida, T., Hohara, Y., Yui, M., Sasaki, N., 1992. Effect of dry density on diffusion of some radionuclides in compacted sodium bentonite. J. Nucl. Sci. Technol. 29, 873–882.

Savage, D., Walker, C., Arthur, R., Rochelle, C., Oda, C., Takase, H., 2007. Alteration of bentonite by hyperalkaline fluids: a review of the role of secondary minerals. Phys. Chem. Earth Parts A/B/C 32, 287–297.

Savage, D., Watson, C., Benbow, S., Wilson, J., 2010. Modelling iron-bentonite interactions. Appl. Clay Sci. 47, 91–98.

Serafeimidis, K., Anagnostou, G., 2014. The Solubilities and thermodynamic equilibrium of anhydrite and gypsum. Rock Mech. Rock. Eng. 48, 15–31.

Steefel, C.I., Lictner, P.C., 1994. Diffusion and reaction in rock matrix bordering a hyperalkaline fluid-filled fracture. Geochim. Cosmochim. Acta 58, 3595–3612.

Steiger, M., 2005a. Crystal growth in porous materials—I: the crystallization pressure of large crystals. J. Cryst. Growth 282, 455–469.

Steiger, M., 2005b. Crystal growth in porous materials—II: influence of crystal size on the

crystallization pressure. J. Cryst. Growth 282, 470–481.
Tachi, Y., Yotsuji, K., 2014. Diffusion and sorption of Cs+, Na+, I− and HTO in compacted sodium montmorillonite as a function of porewater salinity: integrated sorption and diffusion model. Geochim. Cosmochim. Acta 132, 75–93.
Tachi, Y., Yotsuji, K., Suyama, T., Ochs, M., 2014. Integrated sorption and diffusion model for bentonite. Part 2: porewater chemistry, sorption and diffusion modeling in compacted systems. J. Nucl. Sci. Technol. 51, 1191–1204.
Tanaka, S., Noda, N., Higashihara, T., Sato, S., Kozaki, T., Sato, H., Hatanaka, K., 2008. Kinetic behavior of water as migration media in compacted montmorillonite using H218O and applying electric potential gradient. Phys. Chem. Earth Parts A/B/C 33, S163–S168.
Tanaka, S., Noda, N., Sato, S., Kozaki, T., Sato, H., Hatanaka, K., 2011. Electrokinetic study of migration of anions, cations, and water in water-saturated compacted sodium montmorillonite. J. Nucl. Sci. Technol. 48, 454–462.
Techer, I., Bartier, D., Boulvais, P., Tinseau, E., Suchorski, K., Cabrera, J., Dauzères, A., 2012. Tracing interactions between natural argillites and hyper-alkaline fluids from engineered cement paste and concrete: chemical and isotopic monitoring of a 15-years old deep-disposal analogue. Appl. Geochem. 27, 1384–1402.
Tournassat, C., Appelo, C.A.J., 2011. Modelling approaches for anion-exclusion in compacted Na-bentonite. Geochim. Cosmochim. Acta 75, 3698–3710.
Van Loon, L.R., Glaus, M.A., Müller, W., 2007. Anion exclusion effects in compacted bentonites: towards a better understanding of anion diffusion. Appl. Geochem. 22, 2536–2552.
Watson, C., Hane, K., Savage, D., Benbow, S., Cuevas, J., Fernandez, R., 2009. Reaction and diffusion of cementitious water in bentonite: results of 'blind' modelling. Appl. Clay Sci. 45, 54–69.
Wersin, P., Kiczka, M., Koskinen, K., 2016. Porewater chemistry in compacted bentonite: application to the engineered buffer barrier at the Olkiluoto site. Appl. Geochem. 74, 165–175.
Wilson, J.C., Benbow, S., Sasamoto, H., Savage, D., Watson, C., 2015. Thermodynamic and fully-coupled reactive transport models of a steel–bentonite interface. Appl. Geochem. 61, 10–28.
Witten, T.A., Sander, L.M., 1981. Diffusion-limited aggregation, a kinetic critical phenomenon. Phys. Rev. Lett. 47, 1400–1403.
Xu, Y., Yamazaki, M., Villars, P., 2011. Inorganic materials database for exploring the nature of material. Jpn. J. Appl. Phys. 50, 11RH02.
Zheng, L., Samper, J., 2015. Dual-continuum multicomponent reactive transport with nth-order solute transfer terms for structured porous media. Comput. Geosci. 19, 709–726.